PCCP

Accepted Manuscript

ROYAL SOCIETY OF CHEMISTRY

www.rsc.org/pccp

Structural and energetic aspects of the substrate binding and mechanism of action of the DapE-encoded N-succinyl-$_{L,L}$-diaminopimelic acid desuccinylase (DapE) from hybrid QM/MM method

Debodyuti Dutta, and Sabyashachi Mishra*

Department of Chemistry, Indian Institute of Technology Kharagpur, Kharagpur, India

E-mail: mishra@chem.iitkgp.ernet.in

Abstract

With increasing cases of fatal bacterial infections and growing antibiotic resistance, unrelenting efforts are necessary for identification of novel antibiotic targets and new drug molecules. The dapE-encoded N-succinyl-L,L-diaminopimelic acid desuccinylase (DapE), is a di-nuclear Zn containing enzyme in the lysine biosynthetic pathway which is indispensable for bacterial survival and absent in human host, thus a potential antibiotic target. The DapE enzyme catalyzes the hydrolysis of N-succinyl-L,L-diaminopimelic acid (SDAP) to give rise to succinic acid and L,L-diaminopimelic acid. The mechanism of action of the DapE catalyzed SDAP hydrolysis is investigated employing hybrid QM/MM computational method. The DapE side chains, such as, Arg178, Thr325, Asn345 are found to play a role in substrate identification and stabilization in the enzyme active site. Furthermore, a glycine rich loop (Gly322-Ser326) is found to facilitate tight binding of the substrate in the enzyme active site. The catalytic reaction progresses via a general acid-base hydrolysis mechanism where Glu134 first acts as a Lewis base by activating the catalytic water molecule in

the active site, followed by guiding the resulting hydroxyl ion for a nucleophilic attack on the substrate, and finally acts as a Lewis acid by donating a proton to the substrate. The intermediates and transition states along the reaction pathway have been structurally and energetically characterized. A conformational change in the side chain of Asp100, that bridges the two Zn centers of the enzyme, is observed which facilitates the enzymatic action by lowering the activation energy and leads to the formation of a new intermediate during the catalytic reaction. The nucleophilic attack is found to be the rate determining step.

Introduction

Bacterial infections cause millions of death worldwide, thus necessitating constant research efforts to design new antibiotics.[1] Most antibiotics work by interfering with vital cellular functions so as to either kill the bacteria or arrest their multiplication.[2] Currently available antibiotics work on relatively few targets, which tend to be conserved among all bacteria and are highly similar in structure and function.[3] These broad-spectrum antibiotics are likely to become ineffective as bacteria evolve and develop resistance, thus underscoring the importance of identifying novel antibiotic targets and new small molecule inhibitors designed and synthesized to target these enzymes.[4,5]

A biosynthetic pathway that offers promise for the discovery of novel antibiotic targets is the meso-diaminopimelate (mDAP)/lysine biosynthetic pathway.[6–8] This pathway offers several possible antibacterial targets whose potential are yet to be explored.[9,10] The products of this pathway, namely, lysine and mDAP, are inevitable for bacterial growth and multiplication.[11] It has been reported that deletion of the gene encoding for one of the enzymes in the lysine biosynthetic pathway, the dapE-encoded N-succinyl-L,L-diaminopimelic acid desuccinylase (DapE), is lethal to some bacteria.[12,13] Moreover the DapE deletion mutant was unable to grow in lysine-supplemented media, suggesting the importance of DapE for bacterial survival.[14–16] The fact that there are no similar pathways in mammals suggests that inhibitors of

enzymes in the mDAP/lysine pathway may provide selective toxicity against bacteria and spare its human host.[17]

DapE catalyzes the hydrolysis of N-succinyl-L,L-diaminopimelic acid (SDAP) forming L,L-diaminopimelic acid and succinic acid.[6] L,L-diaminopimelic acid serves as the precursor of both mDAP and lysine.[18] The DapE enzymes have been shown to contain dinuclear Zn(II) active sites with a carboxylate (from glutamate) and a histidine residue at each of the two Zn(II) sites which are bridged by a carboxylate group (from aspartate) and a water molecule, (Figure 2a).[14,19] Both metal ions are required for full enzymatic activity which otherwise reduces to 60% with the presence of only one metal ion.[20] Several other metal ions, e.g., Co, Cd, Mn, Ni, Cu, and Mg can also activate DapE to different extent.[20] The relevance of the active site residues have been established by a series of kinetic experiments.[21] While Glu134Asp mutation leaves the Michaelis constant (K_m) unchanged, the k_{cat} decreases by at least three orders of magnitude whereas Glu134Ala mutation completely destroys the catalytic activity.[21] Genes encoding DapEs have been discovered in several multi drug-resistant bacteria suggesting that inhibitors of DapE enzymes may provide a new class of broad-spectrum antibiotics.[6] Therefore, a thorough understanding of the mechanism of action of the DapE enzyme is very important.

While a substantial amount of experimental work has been carried out on DapE, it has received little attention from theory and computation. The hybrid quantum-mechanics and molecular-mechanics (QM/MM) method has been proven exceedingly useful in computational enzymology ever since the pioneering work of Warshel and Levitt in 1976,[22] for which they were awarded the Nobel prize in chemistry in 2013 along with Martin Karplus. A QM/MM method treats the active site in an enzyme, where the process of electronic rearrangement takes place, with QM methods while including the influence of the surrounding protein environment, at the MM level.[23,24]

The present study offers the first computational investigation of the mechanism of action of the DapE enzyme on its natural substrate SDAP. Here we analyze the binding modes of the substrate in the enzyme active site and explore the minimum potential energy pathway through

which the enzyme catalysis takes place. The plausible mechanism of action is schematically represented in Figure 1. In the first step, the substrate binds the enzyme active site, followed by the deprotonation of the catalytic water molecule by Glu134. The resulting hydroxyl ion nucleophile activates the carbon center of the amide carbonyl group of SDAP and gives rise to the tetrahedral intermediate. Finally, the proton transfer from Glu134 to the nitrogen atom of the amide group in SDAP results in the cleavage of the amide C-N bond (Figure 1). The present work is aimed to outline the structural and energetic aspects of the reaction mechanism of DapE enzyme using QM/MM method.

Computational Methods

The X-ray crystallographic structure of DapE (at 2.30 Å resolution) was obtained from the protein data bank (PDB ID: 3IC1)[14] and used as the starting point for all the computational studies. The DapE enzyme exists in a dimeric form with each monomer consisting of a catalytic and dimerization domain. Since the aim of the present work is to study the enzymatic action in the active site, which lies in the catalytic domain, we have considered only the catalytic domain of the monomer A.[14]

With no crystal structure available for the substrate- or inhibitor-bound DapE enzyme complex, the most probable binding mode of the substrate was determined by computationally docking the SDAP substrate to the enzyme active site. Since, only the L,L-isomer is reported to undergo hydrolysis upon binding to the enzyme active site whereas L,D-, D,L-, and D,D-isomers of SDAP remain unactivated by DapE,[18,20] we consider only the L,L stereo-isomer of SDAP for the present study. The L,L-SDAP substrate was docked into the active site of DapE enzyme by using Autodock Tools (version 4.2.3),[25] which employs AMBER force field[26] to estimate the free energy of binding of a ligand to its target. The Merz-Singh-Kollman charge fitting scheme[27] was employed to determine the electrostatic charges on the atoms of both enzyme and substrate for the docking study. Employing genetic algorithm, 50 possible binding poses of

the substrate at the enzyme active site were obtained, where only the ligand was allowed to be flexible while the receptor was kept frozen. The pose with the most favorable binding energy was considered as the most probable binding mode of the substrate.

To account for the conformational degrees of freedom of the receptor with respect to the docked ligand, the docked DapE-SDAP complex was subjected to molecular dynamics simulation. To that end, The enzyme-substrate complex obtained from the docking procedure was immersed in a cubic water box of 90 Å side to ensure that there is a minimum distance of 12 Å between the faces of the box and any atom of the DapE-SDAP complex. The system was made overall charge neutral and a salt concentration of 0.15 M was achieved by adding sodium and chloride ions. The pKa of the titrable side chains in the active site were obtained (Table S1 in the supporting information) from PropKa program.[28] The system was prepared at neutral pH, where all Glu, Asp, Lys, and Arg side chains were modelled as charged, while the His side chains were modelled to be neutral. The system contained 75,820 atoms. To release the bad contacts in the system, first the protein-substrate complex was kept fixed and only the position of the water molecules and that of salt ions were minimized, followed by a full minimization. The system was then slowly heated to 300 K and equilibrated for 2 ns with NVT ensemble at 300 K. The long-range electrostatic interactions were treated by the particle mesh Ewald method with a 12 Å cutoff. The van der Waals interactions were truncated at a cutoff of 12 Å, and a switch function was activated starting at 10 Å. All simulations were performed employing the NAMD program[29] with the CHARMM22 force field,[30] TIP3 potential for water molecules,[31] and Charmm general force field for L,L-SDAP generated from Paramchem suite.[32]

Depending on the schemes employed to evaluate the energetics of the multi-level hybrid systems, the QM/MM methods can be divided into two broad categories, i.e, additive and subtractive.[33] The ONIOM method which employs a subtractive QM/MM scheme to evaluate the energetics of the multi-level system is used in the present work.[34,35] A truncated system was set up for QM/MM calculation by discarding water molecules beyond 8 Å from any solute atom of the protein-ligand complex in the conformation obtained at the end of 2 ns equilibration by

molecular dynamics simulation. The system contained 9900 atoms with 1946 water molecules. A two layer ONIOM[34] method was employed for the QM/MM study of the catalytic mechanism using Gaussian 09 program.[36] The high-level layer (the QM part) consists of 87 atoms that includes two Zn atoms, the catalytic water molecule, side chains of His67, Asp100, Glu134, Glu135, Glu163, His349, and the substrate (LL-SDAP). The bond between C_α and C_β of His and Asp side chains served the boundary between the QM and MM parts, whereas for Glu residues, it was the bond between C_β and C_γ. The valency of C_β atom of His and Asp residues and C_γ atom of Glu residues were fulfilled by hydrogen as link atoms.[37] Both the Zn atoms were considered in +2 oxidation state and the total charge of the high layer is -2. The high level was treated with DFT/6-31G(d,p)[38,39] whereas the MM part of the system was described with AMBER force field.[26]

The reaction was driven along the general acid-base hydrolysis mechanism as shown in Figure 1. For each reaction step, a linear transit scan was carried out for appropriate scan coordinate with reasonably small step size, where the system was subjected to QM/MM optimization at each scan point, employing B3LYP functional[40–42] for the QM region. The entire MM region was subjected to optimization. The highest energy points in the potential-energy curve along the scan coordinate were considered as the starting points for transition state optimization, whereas the minima along the potential-energy curves were considered as the initial guess for the optimization of intermediates of the reaction. Since the entire system is too large for a full frequency calculation, only the 15 lowest modes were calculated to characterize the ground states and transition states. The intermediates have no negative frequencies, and the transition states are characterized by one negative frequency along the reaction coordinate. These optimizations were further carried out employing CAM-B3LYP[43] and M06-2X[44] functionals in addition to the B3LYP functional in order to assess the limitation of B3LYP functional to account for the polarizability of long chains and charge transfer states,[43] which can be crucial to study the enzymatic reactions. At long range the exchange potential behaves as $0.2r^{-1}$, instead of the exact value r^{-1}. CAM-B3LYP overcomes the problem by splitting the interaction

terms between short-range interaction and long-range interaction.[45] Additionally, the M06-2X functional also offers a very good description for non-covalent interactions and charge transfer states important for metalloenzymes.[44]

The QM/MM optimizations were first carried out using the so-called mechanical embedding scheme,[33,35] where the interaction between the high-level and low-level layers are described in MM level which neglects the polarization of charges between different layers. However, when a reaction step progresses, the moieties involved in the reaction change their chemical properties which is reflected in their partial charges at different stages of the reaction. To account for this, the restrained electrostatic potential (RESP)[46,47] program was used to fit partial charges to the electrostatic potential (ESP) grid generated by single point gas phase calculations. After the first optimization using mechanical embedding, the atomic point charges for all the atoms in the QM region were recalculated from a single point QM calculation using the RESP procedure. The resulting structure with improved point charges in QM region was reoptimized using QM/MM method with mechanical embedding.[48] Three cycles of iterations were performed for all intermediates and transition states as well as all the relaxed potential energy scans, to ensure energetic and structural convergence of the optimized structures (Table S5 in the supporting information). The optimized geometry obtained from this self-consistent mechanical embedding scheme was further used for a single point energy calculation with electronic embdding scheme employing[35,49] a higher (6-311+G(d,p)) basis (Table S10 in the supporting information). The self-consistent mechanical embedding scheme employed here has been used in several studies and shown to provide an adequate description of the structure and energy of the system with a significantly lower computational cost.[48,50–54]

In QM/MM optimizations, deciding the size of the QM part is crucial. The QM/MM energy profile is shown to depend on the size of the QM region.[55] The optimized structures, as discussed earlier, contained only one water molecule (the catalytic water) in the QM region (model 1). There are eight additional water molecules that are involved in hydrogen bond network with the side chains of the active site residues. The stationary points, as obtained previously, were

reoptimized with the additional eight water molecules in the QM region (now consisting of 111 atoms) using the three functionals, namely, B3LYP, CAM-B3LYP, and M06-2X discussed earlier. The optimized geometries with the larger QM region (model 2) using B3LYP functionals are discussed in this article, whereas the geometric and energetic details of the stationary points obtained from CAM-B3LYP and M06-2X functionals with model 2 and those of model 1 are reported in the supporting information (Tables S4-S7).

Results and Discussion

The enzyme-substrate complex from docking and MD simulation

The active site of the DapE enzyme exhibits two Zn atoms, bridged by a catalytic water molecule in one side and by the carboxylate side chain of Asp100 on the other (Figure 2a). The side chains of Glu135, Glu163, His67 and His349 show direct coordinations to the active-site Zn atoms. While Zn1 exists in a distorted tetrahedral environment, the Zn2 metal shows a distorted trigonal bipyramidal coordination.[14] In the crystal structure, the Glu134 is strategically positioned near the catalytic water molecule suggesting an important role of activation of the catalytic water molecule (Figure 2a).[14]

The enzyme-substrate complex remains stable during the MD simulations. The plasticity of the apo enzyme was largely preserved during the simulation of the enzyme-substrate complex, as seen from the time series of C_α root mean squared deviation. However, during the equilibration MD simulation, the loop Gly322-Ser326 present between α8 and β12 of the enzyme, shown as red ribbon in Figure 2b, undergoes a large fluctuation from its conformation in the crystal structure, shown as blue ribbon (Figure 2b). This movement in the loop, which is located near the ligand binding site of the enzyme is found to be crucial in allowing a tight binding of the SDAP substrate to the enzyme active site (Figure 2b). The functionally relevant Gly322-Ser326 loop, consisting of GGGTS amino acid sequence, is rich in Gly and Ser residues, which is often associated with rotational freedom of the polypeptide backbone.[56] Such glycine rich segments

are well known to be evolutionarily conserved and are believed to have important functional roles in many microbial proteins.[57–60] The substrate SDAP shows strong coordination with Zn1 via its amide carbonyl group (Zn1-O7 distance is 2.07 Å), and with Zn2 via the carboxylate group of its pimelyl moiety (Zn2-O8 distance is 1.96 Å), see Table 1. In addition to the metal centers, the side chains of the enzyme also exhibit stabilizing interactions with the substrate. The carboxylate group of the succinyl moiety of SDAP is stabilized by an intramolecular hydrogen bond with the amide NH group of SDAP and by an intermolecular hydrogen bonding interaction with the side chain of Asn345 (Figure 2b). While one of the terminal carboxylate groups of the pimelyl moiety of SDAP participates in a salt-bridge interactions with Arg178, the amine group of the pimelyl moiety is stabilized by the side chains of Thr325 (Figure 2b), suggesting a major role of the amine and carboxylate groups of the substrate in identifying the binding site of the enzyme. This observation is in agreement with the experimental finding that the enzyme activity is severely influenced by the presence of the amine and the carboxylate groups of the substrate.[20]

The state of the reactant

The active site of the DapE-SDAP complex obtained from ONIOM QM/MM optimization, is shown in Figure 3. the distance between the two Zn atoms in the optimized structure of the complex is 3.73 Å, as compared to the 3.58 Å in the apo enzyme in the crystal structure, see Table 1. The catalytic water molecule that bridges the two Zn atoms in apo enzyme is pushed towards the Zn1 atom in the enzyme-substrate complex (Zn1-O5 distance is 2.03 Å while Zn2-O5 distance is 3.77 Å). The oxygen atom (O7) of the amide carbonyl group of SDAP is found coordinating to Zn1 (2.06 Å) while it is 2.42 Å away from the Zn2 center (Figure 3). The oxygen atom of the carboxylate group of the succinyl moiety in SDAP, on the other hand, exhibits a strong coordination with Zn2 atom (Zn2-O8 distance is 1.96 Å). The coordination pattern of the two Zn atoms with His67, His349, Glu163, and Asp100, undergo negligible changes upon substrate binding (Table 1). In the apo enzyme, the Glu135 coordinates to the

Zn2 atom with both of its oxygen atoms in the side chain, whereas in the enzyme-substrate complex, Glu135 shows only one coordination with Zn2 atom. The C1-N3 amide bond of SDAP shows a partial double bond character with a bond distance of 1.30 Å. The substrate also exhibits an intramolecular hydrogen bond between the hydrogen atom attached to the nitrogen atom (N3) of the amide group and the oxygen atom (O9) of the terminal carboxylate group of the pimelyl moiety of SDAP (Figure 3).

Activation of the catalytic water molecule

Upon substrate binding, the oxygen atom of the catalytic water molecule makes a stronger coordination with Zn1 center while maintaining a strong inter-molecular hydrogen bond interaction with the carboxylate group of Glu134 (Figure3). In the optimized structure of the DapE-SDAP complex in the reactant state, the distance between H1 of catalytic water and the carboxylate oxygen (O6) of Glu134 is 1.55 Å, which are very favorable distances for an efficient proton transfer from the catalytic water molecule to Glu134. The proton transfer process was further investigated by carrying out a linear transit scan along the O6-H1 distance. The resulting potential energy curve shows that the transfer of proton from the catalytic water molecule to Glu134 involves a barrier at O6-H1 distance of 1.2 Å (Figure 4a). The structure at that point was used as the initial guess of the transition state structure. The active site of the geometry obtained from a transition state optimization of the high-energy structure in the proton transfer process is shown in Figure 5a. The transition state occurs when the proton (H1) is halfway between O5 of catalytic water and O6 of carboxylate oxygen of Glu134, with the O5-H1 and O6-H1 distances of 1.10 and 1.28 Å, respectively (Figure 5a). The activation energy for the formation of TS1 is found to be 2.7 kcal/mol, which indicates an efficient activation of the catalytic water molecule by the DapE enzyme. The optimized geometry of the enzyme-substrate complex in the protonated Glu134 state (IN1) is shown in Figure 5b, is found to be 10.6 kcal/mol more stable than the reactant state. The stable intermediates indicate a greater affinity towards the enzyme and thus provide a tremendous acceleration of the rate of enzymatic action.[61,62]

Nucleophilic attack of the hydroxyl ion on SDAP

In the optimized geometry of IN1, the Glu134 is protonated while the catalytic water results in a hydroxyl ion, which participates in intermolecular hydrogen bonding with the side chains of Glu134 and Glu163 (Figure 5b). The partial charges obtained from the NBO calculation at the optimized geometry of IN1 suggests the most preferable site for nucleophilic attack by the hydroxyl ion is the carbon atom of the amide carbonyl group in the substrate SDAP (Table 2). The nucleophilic attack of the hydroxyl ion is carried out by a linear transit scan along the O5-C1 distance, where C1 is the carbon atom of the amide carbonyl group in SDAP and O5 is the oxygen atom of the hydroxyl ion. The resulting potential energy profile along the scan coordinate shows two maxima at O5-C1 separation of 1.7 Å and 2.4 Å, separated by a minimum at O5-C1 separation of 2.2 Å (Figure 4b). The two high-energy structures were subjected to transition state optimizations to obtain the transition states TS2 and TS3, whereas the low-energy structure was optimized to obtain an intermediate IN2.

The transition state TS2 is 13 kcal/mol above the reactant with O5-C1 distance of 2.37 Å, while retaining the hydrogen bonding interactions between the nucleophile (the hydroxyl ion) and the side chains of Glu134 (Figure 5c). Further progress along the nucleophilic attack results an intermediate (IN2) which is stabilized by 4 kcal/mol with respect to the reactant. Both TS2 and IN2 show a large distance between the metal ions (4.66 and 4.86 Å respectively, Table 1). The large separation of metal centers in TS2 and IN2 is accompanied by a change of coordination of Asp100 with the metal atoms (Figures 5c,d). In TS2 and IN2, the side chain of Asp100 undergoes a conformational change in the form of a rotation of its carboxylate group which results in the breaking of its coordination with Zn2 and thereby disrupting the bridge between the two metal centers. The optimization of stationary points with model 1 exhibits this conformational change of Asp100 occurring only in the IN2 structure. The absence of this conformational change in TS2 is associated with a high energy transition state (TS2) in model 1 (Table S8 in the supporting information). A restrained linear transit scan along O5-C1 distance, by keeping the carboxylate group of Asp100 rigid, resulted in the disappearance of the

intermediate IN2 and the energy of the transition state decreased by 14 kcal/mol as compared to the activation energy from the unrestrained calculation (Figure S1 in the supporting information). This indicates that the conformational change in Asp100 facilitates the enzymatic action by lowering the activation energy of the reaction by allowing the enzyme to follow the minimal free energy path which is not possible in the absence of the degrees of freedom associated with the conformational change of Asp100.

In IN2, the metal center Zn1 is seen coordinating with both the oxygen atoms of Asp100 side chain. It is interesting to note the preference of Asp100 to form two coordination bonds with the Zn1 center which represents the catalytic zinc site that gets preferentially filled by metal ions.[14] Zn2 center on the other hand shows 50% occupancy and the enzyme can be activated even in the absence of Zn2 atom.[14] Similar flexibility of the metal sites is also reported in other dinuclear enzymes where the enzyme activity is promoted by conformational changes at the metal sites.[63] In the IN2 state, both the Zn centers show tetra-coordination. The coordination between Zn and the enzyme side chains are the strongest in IN2, as can be seen from the reduced bond distances between Zn1 with O1 (Glu163), O3 (Asp100), O4 (Asp100), N1 (His67) and Zn2 with O2 (Glu135), N2 (His349), O8 (SDAP), O7 (SDAP), see Table 1. The intermediate IN2 arising from the flexibility of the metal centers and the Asp100 side chain, emphasizes the role of conformational dynamics in enzyme catalysis[61,62,64–67]

During the course of the nucleophilic attack, the intermediate state IN2 leads to the formation of a second transition state (TS3) 14.6 kcal/mol above the reactant and at the nucleophile-electrophile (O5-C1) distance of 1.65 Å (Figure 5e) Along the IN2 to TS3 part of the nucleophilic attack, the Asp100 bridge between the two Zn atoms is restored and the intermetalic distance decreases to 3.66 Å in TS3. At the TS3 state, the amide carbonyl group of SDAP develops single bond character, as seen by the elongated C1-O7 bond (Table 1 and Figure 5e).

The transition state TS3 yields the tetrahedral intermediate (TD), which is about 10.2 kcal/mol more stable than the reactant. In this state, the carbon atom (C1) of the amide carbonyl center in SDAP is bonded to two oxygen atoms by single bonds and the corresponding NBO analysis

shows an sp^3 hybridisation for C1. The NBO analysis shows a partial charge of -1 on O7 atom which arises due to the concentration of the π cloud of C1-O7 double-bond over O7 atom after the nucleophilic attack on C1 (see Table 2). In addition, the partial double bond character of the amide C1-N3 bond develops a single bond character in the TD intermediate (Figure 5f), where a C1-N3 distance of 1.49 Å is seen compared to 1.30 Å in the reactant state (Table 1) The TD intermediate state exhibits several changes in the hydrogen bond network near the active site. In this state, the intra-substrate hydrogen bond between the hydrogen attached to the amide nitrogen atom (N3) and the O9 atom of the terminal carboxylate group of SDAP is replaced by another intra-substrate hydrogen bond between O9 atom and the hydroxyl group attached to the C1 of the substrate (O9-H2 separation 1.41 Å, Figure 5f). Furthermore, the tetrahedral intermediate (TD) shows a new intermolecular hydrogen bond between the N3 atom (with a highly negative partial charge, Table 2) and the protonated Glu134 (N3-H1 separation 1.59 Å, Figure 5f).

Proton transfer from Glu134 to the substrate

The strong electrostatic interaction between the protonated Glu134 and NH group of SDAP and the weakening of the amide bond (C1-N3) in the intermediate TD (Figure 5f), provide an ideal platform for the breaking of the C1-N3 amide bond which is facilitated by a proton transfer from Glu134 to the NH group of the substrate. The energy profile for the relaxed potential energy scan along the proton-transfer coordinate is shown in Figure 4c. The structure corresponding to N3-H1 distance of 1.3 Å was used for a transition state optimization which resulted in the transition state (TS4) about 6 kcal/mol above TD and 4.3 kcal/mol below R. In TS4, the transferred proton is 1.30 Å from the proton-donor (O6 of Glu134) and 1.24 Å from the proton acceptor (N3 of substrate), see Figure 5g. The C1-O7 single bond in the TD state starts developing a partial double bond character in TS4 leading to a C1-O7 distance of 1.35 Å and the C1 center regains its sp^2 character which results in the weakening of C1-N3 bond (1.57 Å).

The transition state TS4 leads to the product state (P) which is found to be 13 kcal/mol

more stable compared to the reactant state. The optimized geometry of the product state shows the cleaved amide bond with a C1-N3 distance of 2.74 Å (Figure 5h). In the product state, Glu134 is deprotonated while the SDAP substrate is decomposed into a succinic acid fragment and diamine pimelic acid fragment.

The role of active site water molecules, the density functionals, and the QM/MM scheme in the reaction energetics

In the equilibrated structure of DapE-SDAP complex, the side chains of Glu134, Glu135, Glu163, Asp100 in the active site of the enzyme are stabilized by solvent water molecules. To investigate the role of these water molecules in the reaction energetics, the energy profiles of the enzymatic reaction were obtained by treating these water molecules in MM region (model 1) and in QM region (model 2). The optimized geometries of the stationary points from both the models are compared in the supporting information (Tables S4-S7). The structural changes in the optimized geometries of the intermediates and transition states obtained from the two models are marginal, varying between RMSD values of 0.05 Å to 0.8 Å (Table S9, in the supporting information). However, the energetics of the catalytic reaction is poorly described when the water molecules in the active site are treated classically (model 1). A very high activation energy of 36.4 kcal/mol is obtained in the absence of the active site water molecules in the QM region, as compared to 23.6 kcal/mol when they are included in the QM region (with the B3LYP functional).

To evaluate the role of the density functionals in the energetics of the reaction, the intermediates and the transition states were optimized using three different functionals, namely, B3LYP, CAM-B3LYP, and M06-2X, for both model 1 and model 2. Activation energy barrier (corresponding to the formation of TS2 transition state) of 36.4, 27.6, and 26.7 kcal/mol, for the B3LYP, CAM-B3LYP, and M06-2X functionals, respectively, were obtained for the model 1 (Table S8 in the supporting information). On the other hand, when the active site water

molecules were treated within QM region (model 2), an activation energy of 23.7, 22.2, 19.9 kcal/mol were obtained for the B3LYP, CAM-B3LYP, and M06-2X functionals, respectively. For a given QM/MM model, the energetics of the reaction is not found to be significantly altered by the three functionals employed here. On the contrary, the model 2 with active site water molecules in the QM region obtained a lower activation energy for all three functionals. In particular, the model 2 with the M06-2X functional provides the activation energy barrier of 19.9 kcal/mol, which is in very good agreement with the experimental value of the free energy of activation of 15.2 kcal/mol.[20]

We have studied the energetics of the enzymatic reaction by employing the self-consistent mechanical embedding approach where the partial charges of the QM region are iteratively improved until convergence.[48] This method has been used in several QM/MM studies to describe reaction in complex systems,[48,50–54] with a much reduced computational cost compared to the standard electronic-embedding scheme.[35,49] We have performed benchmark calculations to show the validity of the self-consistent mechanical embedding approach as compared to the electronic-embedding scheme.

To this end, we have carried out single point energy calculations with 6-311+G(d,p) basis set employing electronic embedding scheme on the optimized geometry obtained from the self-consistent mechanical embedding scheme for all the intermediates and transition states. The difference in energy between these two sets of calculations (Table S10 in the supporting information) are found to be very small with a maximum energy difference of 1.6 kcal/mol and RMSD of the energy over the nine intermediates and transition states is 0.25 kcal/mol. We have also optimized the structures obtained from the self-consistent mechanical embedding optimization by employing electronic embedding method, for the reactant, the transition state TS2, tetrahedral intermediate, and the product. The results (shown in Table S11 in the supporting information) indicate that the optimization with the electronic embedding scheme results in an energy difference of 0.21, 2.78, 0.75, and 1.12 kcal/mol for the reactant, TS2, tetrahedral intermediate, and the product, respectively, while the same for the structural change (in terms

of RMSD) are 0.04, 0.06, and 0.05, and 0.08 Å, respectively. Furthermore, the atomic partial charges determined from NBO calculations of the optimized geometries obtained from the self-consistent mechanical embedding scheme and the electronic embedding scheme exhibit an excellent agreement (see Table S12 in the supporting information). This analysis clearly suggests that the self-consistent mechanical embedding scheme employed in this work captures the structural and energetic aspects of the enzymatic reaction accurately.

Conclusion

DapE, a crucial enzyme in the lysine biosynthetic pathway, is a promising antibiotic target. In the present work, a detailed account of the binding and DapE-catalyzed hydrolysis of the L,L-SDAP substrate is obtained by employing computational methods.

The substrate L,L-SDAP is found to coordinate to the two Zn atoms in the active site via its carboxylate group of the pimelyl moiety and the amide carbonyl group. The substrate recognition and stabilization is contributed by the side chains of Arg178, Thr325, and Asn345 in DapE. The glycine rich loop (Gly322-Ser326) present between α8 and β12 of DapE facilitates a tight binding of the substrate in the enzyme active site by undergoing loop movement. In several other microbial enzymes, highly conserved glycine rich segments have important functional roles.[57–60] The functional and evolutionary role of the glycine rich loop in the DapE enzyme is hoped to be further probed with appropriate mutants of the enzyme.

The substrate hydrolysis is studied by dividing the reaction in to three steps. In the first step, Glu134 activates the catalytic water molecule by acting as a proton acceptor. This step involves a rather small activation energy barrier (2.7 kcal/mol). The resulting hydroxyl ion carries out a nucleophilic attack on the amide carbonyl group of the substrate in the second step. The nucleophilic attack takes place via two transition states separated by an intermediate. During the nucleophilic attack, a conformational change in the binding mode of the Asp100 to the two Zn atoms results the intermediate. By adopting this conformational change, the enzyme

explores the minimal free energy path that lowers the activation energy barrier. It is hoped that the present work will inspire experimental verification of this conformational change. After the nucleophilic attack, a proton is transferred from Glu134, which played the role of a base in the first step, to the amide N atom of the substrate which results in the cleavage of the amide bond and completes the hydrolysis of the substrate. The final step involves a small activation energy barrier of 6 kcal/mol. Overall, the QM/MM calculations predict the nucleophilic attack as the rate determining step with an activation energy barrier of 23.7 kcal/mol, 22.2 kcal/mol, and 19.9 kcal/mol, by employing B3LYP, CAM-B3LYP, and M06-2X functionals, respectively, as compared to the experimental value of the free energy of activation of 15.2 kcal/mol.[20] The agreement with experiment is reasonable given the fact that in the present work the activation barriers represent only the enthalpic contribution and they do not account for the entropic contributions. The treatment of water molecules in the active site region by quantum mechanics was found to be very important in describing the energetics of the overall reaction, which accounted for a lowering of the activation energy barrier by 6 to 12 kcal/mol, depending on the density functional employed.

The present work suggests a very important role of Glu134 in the substrate hydrolysis. While Glu134 does not participate in binding and stabilizing the substrate, it acts as a Lewis base and a Lewis acid at different stages of the reaction. This explains the little change in K_m value for the Glu134Asp mutant. In addition, Glu134 participates in a strong hydrogen bonding interaction with the nucleophile (the hydroxyl ion) throughout the nucleophilic attack, thereby providing a platform for an efficient nucleophilic attack. When Glu134 is replaced by Asp, the length of the side chain decreases by one methyl unit. This prevents Asp134 to stabilize the nucleophile to the same extent as is done by Glu134, which explains the lowering of k_{cat} value for substrate hydrolysis by three orders of magnitude for Glu134Asp mutant.[21] When Glu134 is mutated by Ala, the loss of the ability to accept or donate proton leads to complete destruction of the enzyme activity.[21]

In summary, we have provided the structural and energetic characterization of the mecha-

nism of action of DapE in terms of the intermediates and transition states. The future investigation of the mechanism of action with different mutants of the enzyme and with different metal centers will further increase our understanding of the action of the DapE enzyme which holds a bright future towards the design and development of novel antibacterial drugs.

Table 1: Geometric characterization of the active site of DapE during its enzymatic action on SDAP. The important bond distances (in Å) in the active site of DapE crystal structure (C) and in the critical points during the hydrolysis of SDAP by DapE are given in Å. The reactant state, the tetrahedral intermediate, and the product states are referred as R, TD, and P, respectively. TS1 through TS4 represent four transition states while IN1 and IN2 represent two intermediates observed during the QM/MM study of the reaction. The coordination number (CN) of both the Zn atoms are shown for the crystal structure, all intermediates, and transition states.

Bond	**C**	**R**	**TS1**	**IN1**	**TS2**	**IN2**	**TS3**	**TD**	**TS4**	**P**
Zn1-Zn2	3.58	3.73	3.63	3.98	4.66	4.86	3.66	3.47	3.54	3.65
Zn2-O2(E135)	1.99	1.99	1.94	1.97	2.71	2.10	1.97	1.92	1.96	1.95
Zn1-O1(E163)	2.05	2.00	1.96	2.05	2.04	2.06	2.06	1.94	2.01	2.03
Zn2-O4(D100)	1.97	1.99	2.00	2.08	3.63	3.87	2.10	2.08	2.08	2.08
Zn1-O3(D100)	2.01	2.01	2.01	1.93	1.95	1.97	1.98	1.96	1.98	1.98
Zn2-N2(H349)	2.22	2.08	2.10	2.11	2.08	2.04	2.11	2.14	2.16	2.14
Zn1-N1(H67)	2.15	2.21	2.18	2.07	2.06	2.07	2.11	2.09	2.10	2.04
Zn2-O5(WAT)	2.12	3.77	3.64	3.50	3.92	3.91	4.13	4.12	4.17	4.43
Zn1-O5(WAT)	2.22	2.03	1.95	1.90	2.00	1.81	2.30	2.59	2.62	3.01
H1(WAT)-O5(WAT)		1.01	1.10	1.39	1.46	1.63	1.95	3.06	2.88	3.06
H2(WAT)-O5(WAT)		0.97	0.97	0.96	0.96	0.96	0.96	1.03	1.06	1.04
H1(WAT)-O6(E134)		1.55	1.28	1.03	1.04	1.01	1.02	1.04	1.30	2.80
H2(WAT)-O9(SDAP)		6.85	6.73	5.56	4.45	4.46	4.16	1.49	1.41	1.50
C1(SDAP)-N3(SDAP)		1.30	1.30	1.32	1.32	1.33	1.36	1.49	1.57	2.74
C1(SDAP)-O5(WAT)		3.93	3.85	3.67	2.37	2.21	1.65	1.38	1.37	1.35
C1(SDAP)-O7(SDAP)		1.28	1.27	1.26	1.27	1.27	1.37	1.39	1.39	1.28
H1(WAT)-N3(SDAP)		4.38	4.17	5.00	3.49	3.46	3.23	1.59	1.24	1.01
Zn2-O8(SDAP)		1.96	1.99	2.01	1.92	1.98	2.03	2.09	2.11	2.01
Zn1-O8(SDAP)		2.42	2.19	2.03	1.91	1.91	2.03	1.97	2.02	2.26
Zn1-O7(SDAP)		2.06	2.13	3.37	3.34	3.47	2.01	1.93	1.94	2.01
CN of Zn2	5	4	4	5	4	4	5	5	5	5
CN of Zn1	4	5	5	4	4	4	5	4	4	4

Table 2: Partial charges obtained from NBO analysis at the QM/MM optimized geometries corresponding to the critical points during the hydrolysis of SDAP by DapE.

Atoms	**R**	**TS1**	**IN1**	**TS2**	**IN2**	**TS3**	**TD**	**TS4**	**P**
Zn1	1.310	1.308	1.307	1.304	1.284	1.320	1.302	1.315	1.314
Zn2	1.313	1.312	1.297	1.293	1.307	1.307	1.304	1.308	1.307
O1(E163)	-0.809	-0.809	-0.800	-0.778	-0.798	-0.799	-0.811	-0.815	-0.816
O2(E135)	-0.839	-0.839	-0.815	-0.811	-0.829	-0.814	-0.817	-0.817	-0.819
O3(D100)	-0.746	-0.743	-0.767	-0.783	-0.811	-0.789	-0.782	-0.776	-0.774
O4(D100)	-0.789	-0.790	-0.757	-0.736	-0.693	-0.733	-0.738	-0.749	-0.758
O5(WAT)	-1.096	-1.122	-1.152	-1.125	-1.086	-0.918	-0.822	-0.816	-0.809
O6(E134)	-0.773	-0.759	-0.742	-0.760	-0.741	-0.714	-0.719	-0.744	-0.760
N1(H67)	-0.551	-0.546	-0.563	-0.584	-0.599	-0.598	-0.582	-0.593	-0.600
N2(H349)	-0.593	-0.591	-0.580	-0.588	-0.603	-0.581	-0.587	-0.583	-0.587
H1(WAT)	0.531	0.529	0.533	0.529	0.532	0.546	0.540	0.501	0.489
H2(WAT)	0.514	0.508	0.495	0.491	0.493	0.502	0.517	0.515	0.515
O7(SDAP)	-0.797	-0.796	-0.768	-0.794	-0.789	-0.913	-0.988	-0.856	-0.769
O8(SDAP)	-0.828	-0.826	-0.815	-0.804	-0.829	-0.801	-0.787	-0.784	-0.791
C1(SDAP)	0.729	0.730	0.729	0.754	0.770	0.744	0.778	0.791	0.809
N3(SDAP)	-0.618	-0.619	-0.622	-0.628	-0.679	-0.749	-0.768	-0.729	-0.725

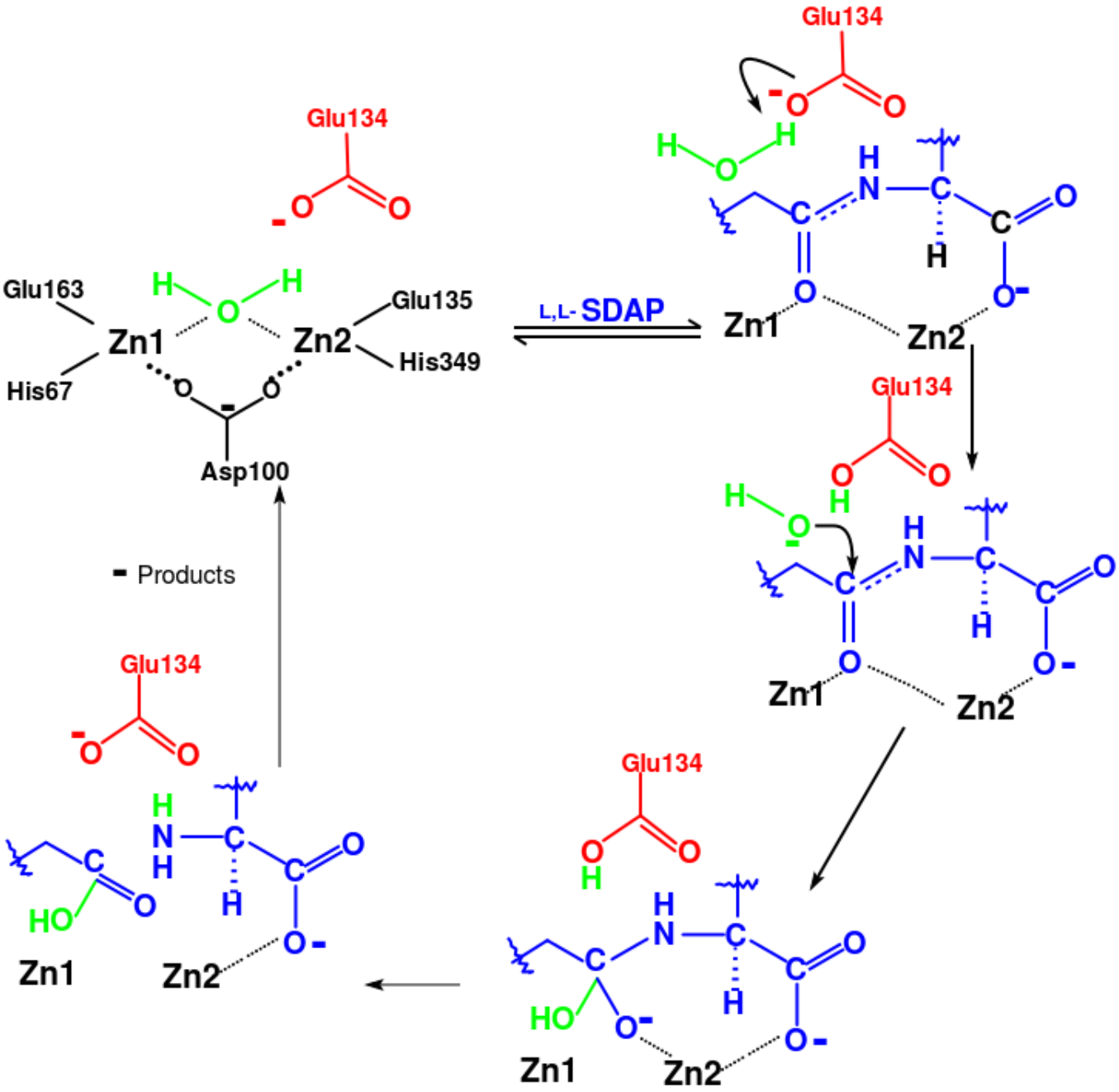

Figure 1: Putative mechanism of the hydrolysis of L,L-SDAP by DapE.

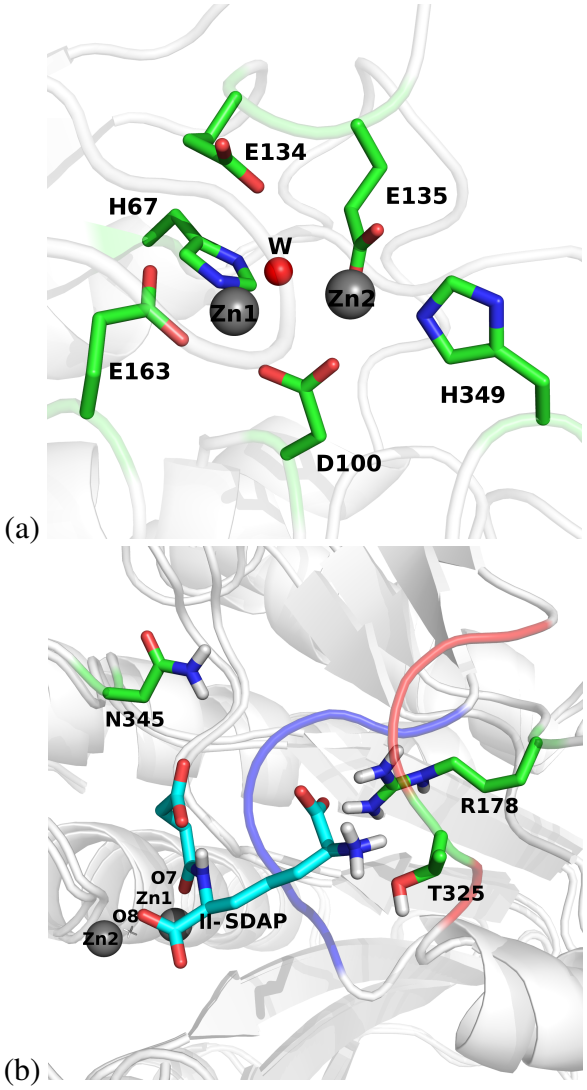

Figure 2: (a) The active site of the DapE enzyme showing the Zn atoms, catalytic water molecule, and the side chains of the active site residues. The protein backbone is shown as ribbons. The residues shown in stick representation show C, H, N, O, Zn atoms in green, white, blue, red, and gray, respectively. The same color scheme is followed in all figures. (b) The SDAP substrate in the active site of DapE after 2 ns of equilibration of the enzyme-substrate complex. The C atoms of substrate are shown in cyan for clarity. The substrate coordination to the Zn atoms and substrate stabilization by Arg178, Thr325, and Asn345 side chains are highlighted. The backbone of the apo enzyme from the crystal structure is overlaid for comparison with the equilibrated conformation of the enzyme-substrate complex. The large fluctuation of the loop Gly322-Ser326 during the enzyme-substrate equilibration (shown as red ribbon) can be seen when compared to its crystal structure conformation (blue ribbon).

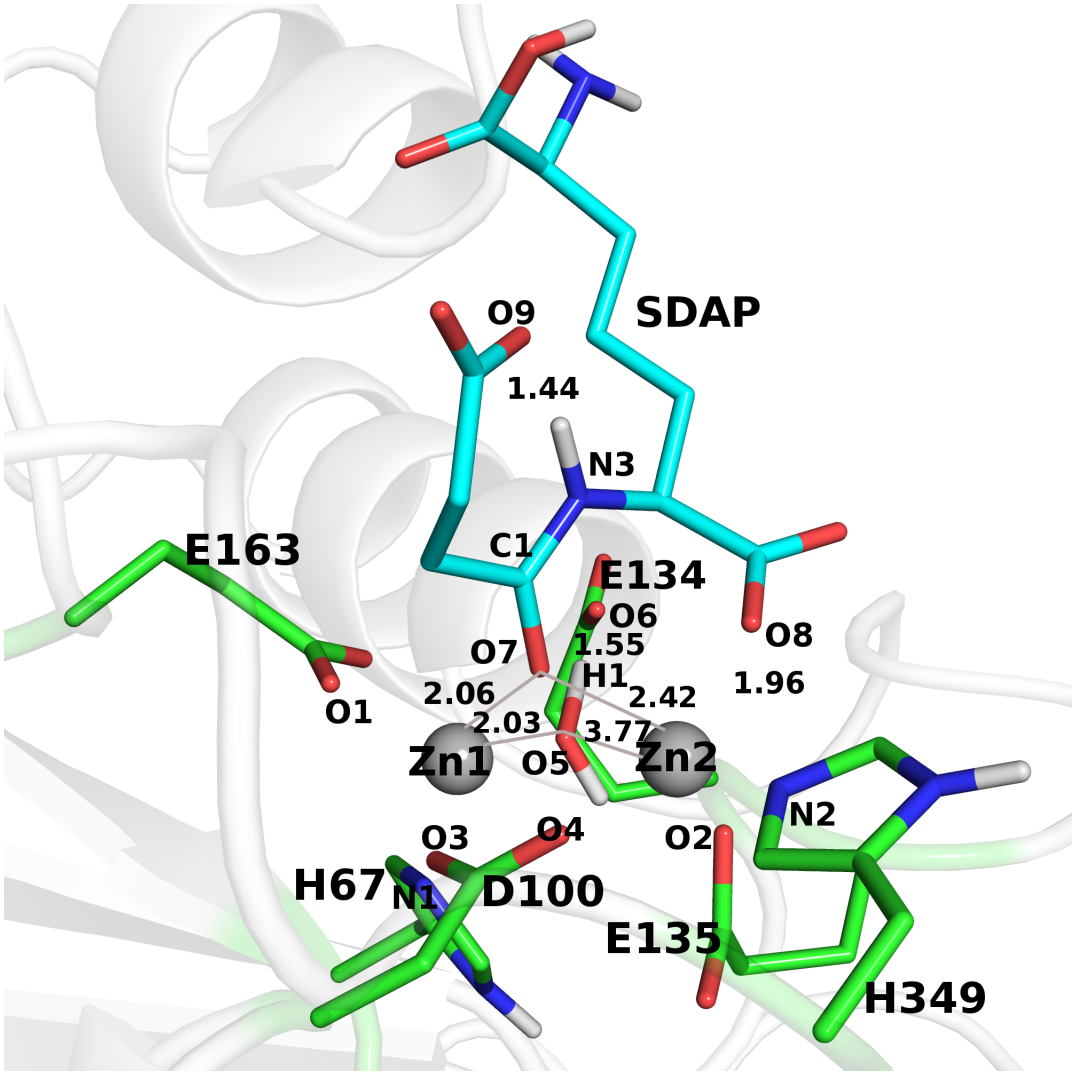

Figure 3: The active site of the DapE-SDAP complex in the reactant state (R) obtained from ONIOM QM/MM optimization. The carbon atoms of SDAP are shown in cyan for clarity. The important atoms are numbered and the numbering scheme is followed throughout. The distances are in Å.

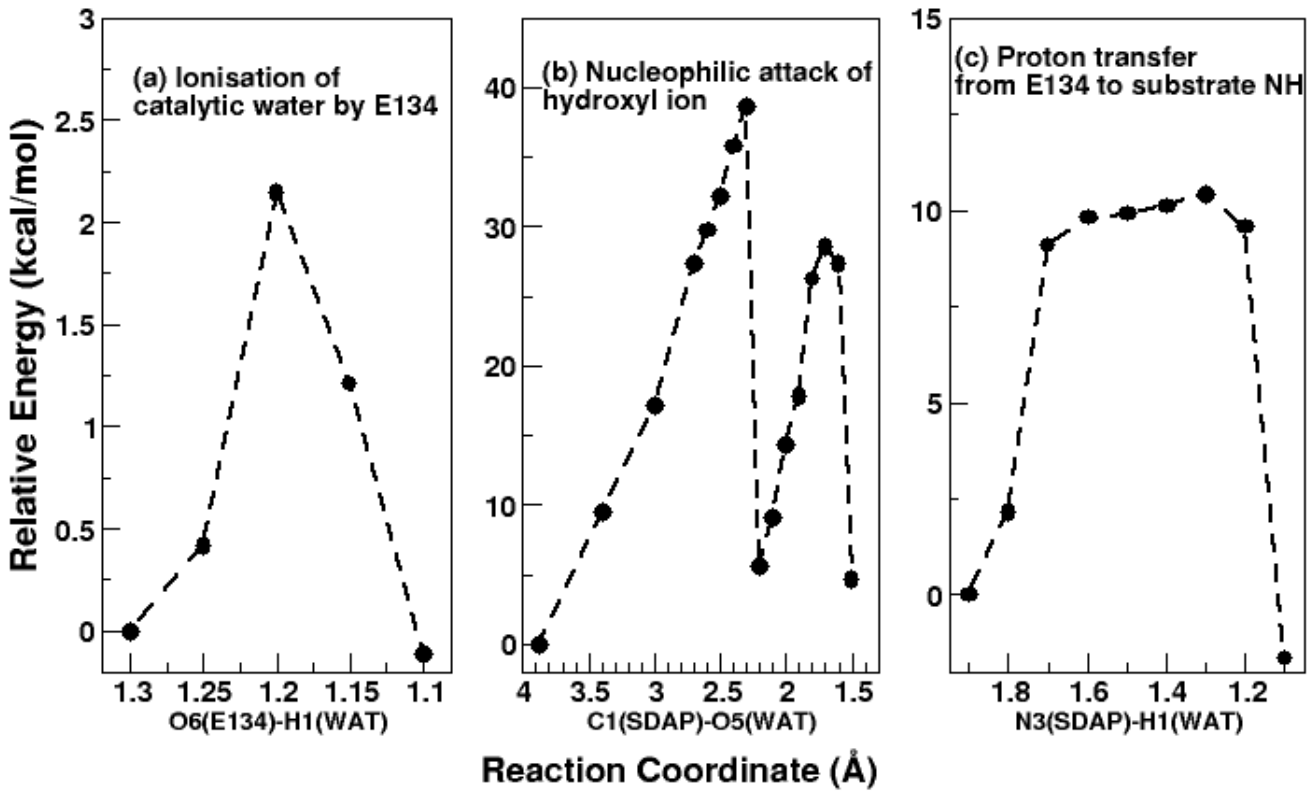

Figure 4: The potential energy profiles obtained from linear transit (relaxed) scan of the potential energy surface along the reaction coordinates.

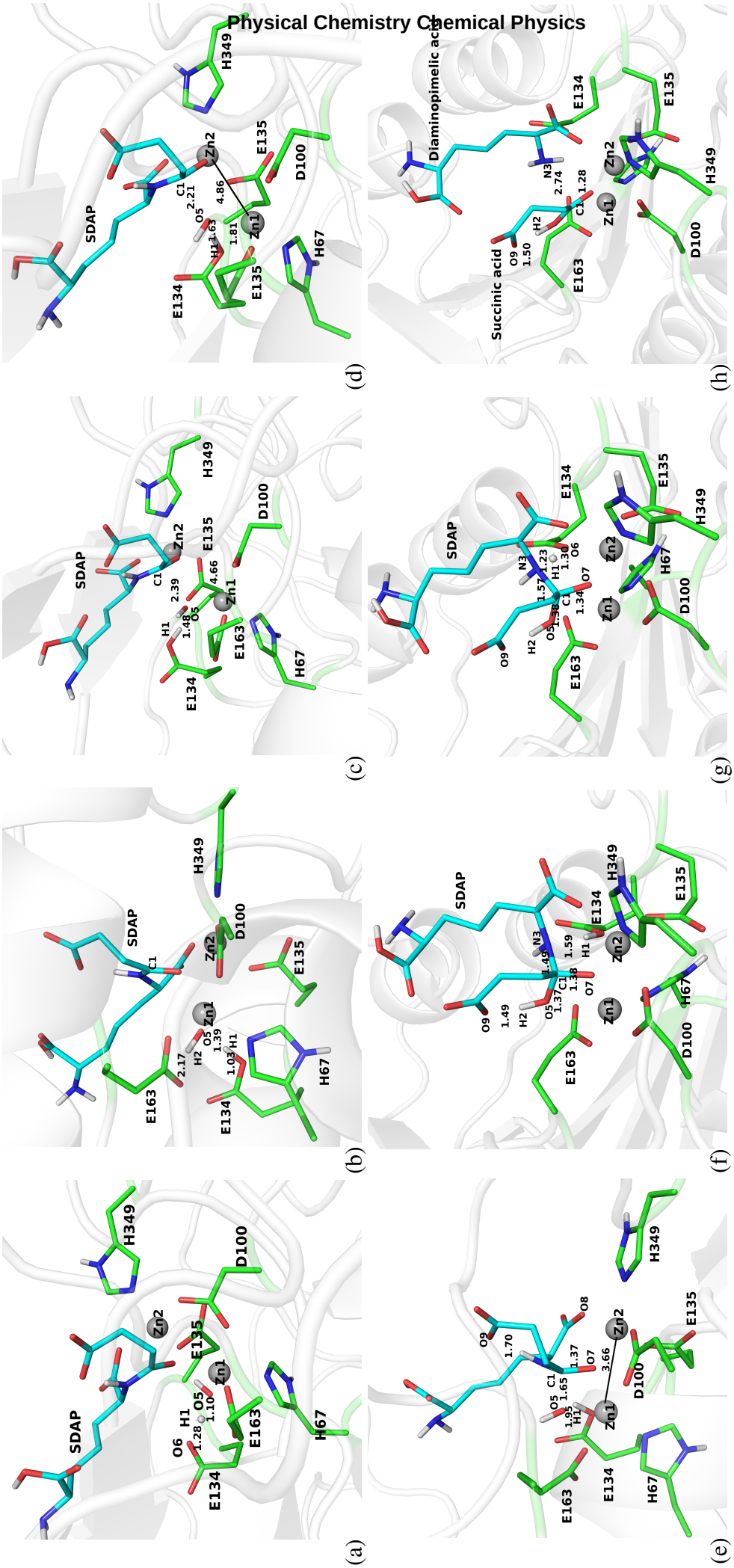

Figure 5: The optimized geometry of the transition states, intermediates, and final product during SDAP hydrolysis by DapE enzyme. The structures shown in (a) through (h) correspond to the TS1, IN1, TS2, IN2, TS3, TD, TS4, and P, respectively, obtained from B3LYP functional employed in model 2 (111 atoms in the QM region). The distances are in Å.

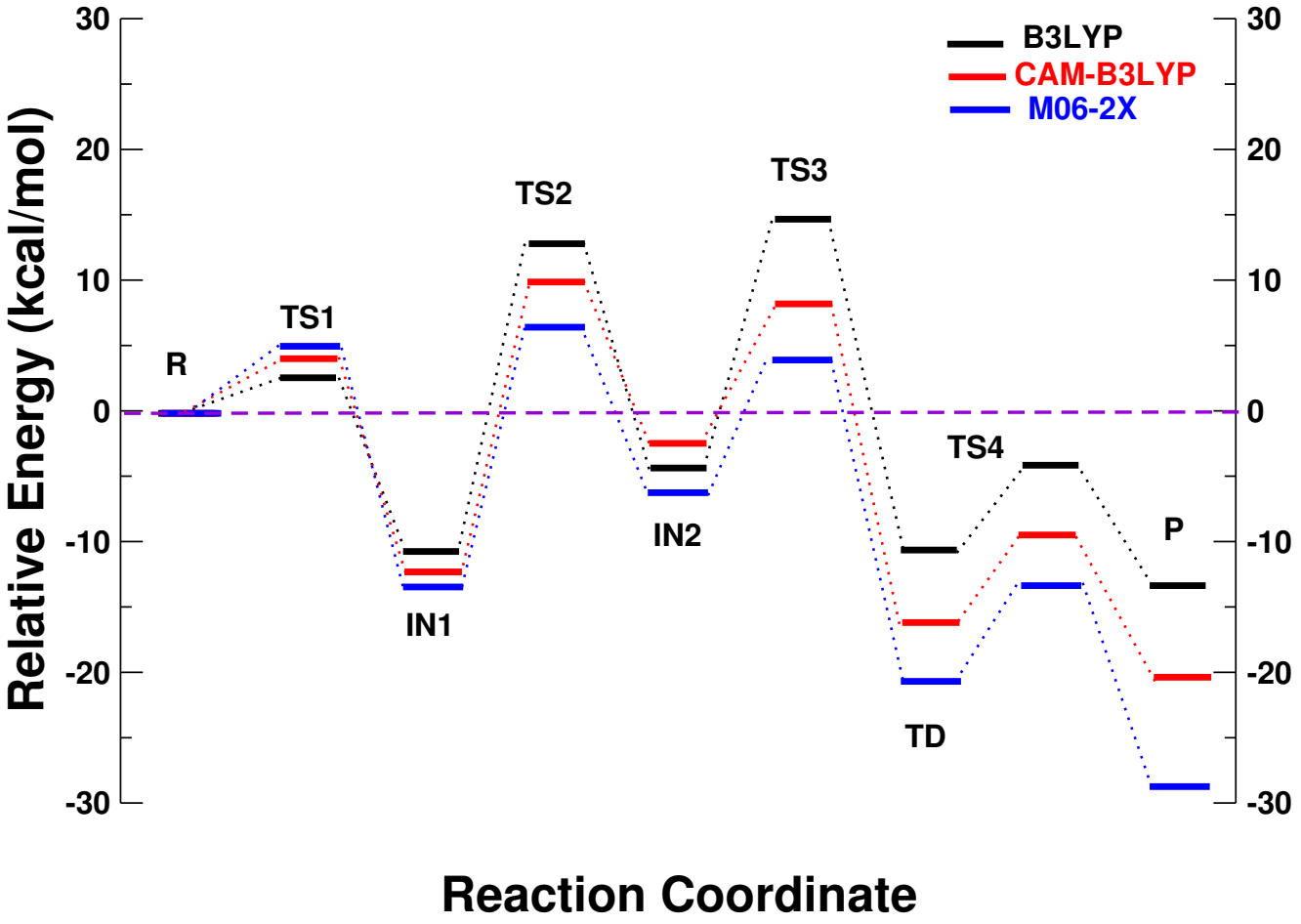

Figure 6: The energy profile diagram of hydrolysis of SDAP by DapE enzyme. The energy of the DapE-SDAP reactant state is used as reference energy.

Acknowledgement

The authors thank Dr. Marc Creuss for valuable suggestions on the manuscript. SM thanks DST-India, New Delhi for Ramanujan Fellowship and IIT Kharagpur for ISIRD grant.

Supporting Information Available

Supporting information Available: Optimized geometries of the intermediates and transition states in Cartesian coordinates, some additional tables and figures, and complete citation for ref.[36]

Table of Contents Graphics

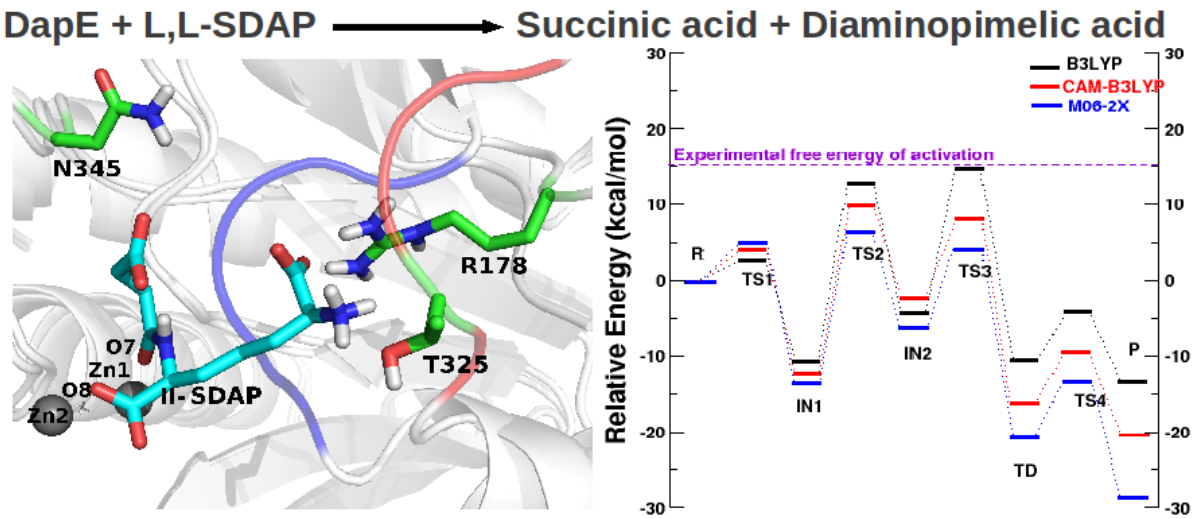

Substrate binding and mechanism of action of the DapE-encoded

N-succinyl-L,L-diaminopimelic acid desuccinylase (DapE)

REFERENCES

(1) Donadio, S.; Maffioli, S.; Monciardini, P.; Sosio, M.; Jabes, D. *The Journal of Antibiotics* **2010**, *63*, 423–430.

(2) Davies, J.; Davies, D. *Microbiol. Mol. Biol. Rev.* **2010**, *74*, 417–433.

(3) Wilke, M. S.; Lovering, A. L.; Strynadka, N. C. J. *Curr. Opin. Microbiol.* **2005**, *08*, 525–533.

(4) Levy, S. B.; Marshall, B. *Nat. Med.* **2004**, *10*, 122–129.

(5) Coates, A.; Hu, Y.; Bax, R.; Page, C. *Nat. Rev. Drug. Discov.* **2002**, *1*, 895âĂŞ910.

(6) Holz, R. C.; Bienvenue, D. L.; Gilner, D. M.; Davis, R. S.; Bennett, B. *Biochemistry* **2003**, *42*, 10756–10763.

(7) Uda, N.; Upert, G.; Angelici, G.; Nicolet, S.; Schmidt, T.; Schwede, T.; Creus, M. *Metallomics* **2014**, *6*, 88–95.

(8) Usha, V.; Lloyd, A.; Lovering, A.; Besra, G. *FEMS. Microbiol. Lett.* **2012**, *330*, 10–16.

(9) Gillner, D.; Armoush, N.; Holz, R.; Becker, D. *Bioorg. Med. Chem. Lett.* **2009**, *19*, 6350–6352.

(10) Girodeau, J. M.; Agouridas, C.; Masson, M.; LeGoffic, F. *J. Med. Chem.* **1986**, *29*, 1023–1030.

(11) Karita, M.; Etterbeek, M. L.; Forsyth, M. H.; Tummuru, M. R.; Blaser, M. J. *Infect. Immun.* **1997**, *65*, 4158–4164.

(12) Pavelka, M.; Jacobs, W. *J. Bacteriol.* **1996**, *178*, 6496–6507.

(13) Velasco, A. M.; Leguina, J. I.; Lazcano, A. *J. Mol. Evol.* **2002**, *55*, 445–459.

(14) Nocek, B.; Gillner, D.; Fan, Y.; Holz, R.; Joachimiak, A. *J. Mol. Biol.* **2010**, *397*, 617–626.

(15) Scapin, G.; Blanchard, J. S. *Adv. Enzymol.* **1998**, *72*, 279–325.

(16) Born, T. L.; Blanchard, J. S. *Curr. Opin. Chem. Biol* **1999**, *3*, 607–613.

(17) Gillner, D.; D.P., B.; Holz, R. *J. Biol. Inorg. Chem.* **2013**, *13*, 155–163.

(18) Born, T. L.; Zheng, R.; Blanchard, J. S. *Biochemistry* **1998**, *37*, 10478–10487.

(19) Cosper, N.; Bienvenue, D.; Shokes, J.; Gilner, D.; Tsukamoto, T.; Scott, R.; Holz, R. *J. Am. Chem. Soc.* **2003**, *125*, 14654–14655.

(20) Bienvenue, D.; Gillner, D.; Davis, R.; Bennett, B.; Holz, R. *Biochemistry* **2003**, *42*, 10756–10763.

(21) Davis, R.; Bienvenue, D.; Swierczek, S.; Gillner, D.; Rajagopal, L.; Bennett, B.; Holz, R. *J. Biol. Inorg. Chem.* **2006**, *11*, 206–216.

(22) Warshel, A.; Levitt, M. *J. Mol. Biol.* **1976**, *103*, 227–249.

(23) Bakowies, D.; Thiel, W. *J. Phys. Chem.* **1996**, *110*, 10580–10594.

(24) Lin, H.; Truhlar, D. G. *Theor. Chem. Acc.* **2007**, *117*, 185âĂŞ199.

(25) Morris, G. M.; Goodsell, D. S.; Halliday, R. S.; Huey, R.; Hart, W. E.; Belew, R. K.; Olson, A. J. *J. Comput. Chem.* **1998**, *19*, 1639–1662.

(26) Weiner, P. K.; Kollman, P. A. *J. Comput. Chem.* **1981**, *2*, 287–303.

(27) Singh, U. C.; Kollmann, P. *J. Comput. Chem.* **1984**, *5*, 129–145.

(28) Sondergaard, C. R.; Olsson, M. H. M.; Rostkowski, M.; Jensen, J. H. *J. Chem. Theory Comput.* **2011**, *7*, 2284–2295.

(29) Phillips, J. C.; Braun, R.; Wang, W.; Gumbart, J.; Tajkhorshid, E.; Villa, E.; Chipot, C.; Skeel, R. D.; Kale, L.; Schulten, K. *J. Comput. Chem.* **2005**, *26*, 1781–1802.

(30) Foster, J. P.; Weinhold, F. *J. Phys. Chem. B* **1998**, *102*, 3586–3616.

(31) Jorgensen, W. L.; Madura, J. D. *J. Am. Chem. Soc.* **1983**, *105*, 1407–1413.

(32) Vanommeslaeghe, K.; Hatcher, E.; Acharya, C.; Kundu, S.; Zhong, S.; Shim, J.; Darian, E.; Guvench, O.; Lopes, P.; Vorobyov, I.; MacKerell, A. D., Jr. *J. Comput. Chem.* **2010**, *31*, 671–690.

(33) Senn, M. H.; Thiel, W. *Angew. Chem. Int. Ed.* **2009**, *48*, 1198–1229.

(34) Dapprich, S.; Komaromi, I.; Byun, K.; Morokuma, K.; Frisch, M. J. *Journal of Molecular Structure (Theochem)* **1999**, *461*, 1–21.

(35) Vreven, T.; Byun, K. S.; Komaromi, I.; Dapprich, S.; Montgomery, J. A., Jr.; Morokuma, K.; Frisch, M. J. *J. Chem. Theory Comput.* **2006**, *2*, 815–826.

(36) Frisch, M. J. et al. *Gaussian 09 Revision A.1*, Gaussian Inc. Wallingford CT 2009.

(37) Reuter, N.; Dejaegere, A.; Maigret, B.; Karplus, M. *J. Phys. Chem. A* **2000**, *104*, 1720–1735.

(38) Ditchfield, R.; Hehre, W. J.; Pople, J. A. *J. Chem. Phys.* **1971**, *54*, 724–729.

(39) Rassolov, V. A.; Ratner, M. A.; Pople, J. A.; Redfern, P. C.; Curtiss, L. A. *J. Comput. Chem.* **2001**, *22*, 976–984.

(40) Becke, A. *J. Phys. Chem. B* **1993**, *98*, 5648–5652.

(41) Lee, C.; Yang, W.; Parr, R. *Phys. Rev. B* **1988**, *37*, 785–789.

(42) Becke, A. *Phys. Rev. A* **1988**, *38*, 3098âĂŞ3100.

(43) Yanai, T.; Tew, D. P.; Handy, N. C. *Chem. Phys. Lett.* **2004**, *393*, 51–57.

(44) Zhao, Y.; Truhlar, D. G. *Theor. Chem. Acc.* **2008**, *120*, 215–241.

(45) Iikura, H.; Tsuneda, T.; Yanai, T.; Hirao, K. *J. Chem. Phys.* **2001**, *115*, 3540–3548.

(46) Bayly, C. I.; Cieplak, P.; Cornell, W.; Kollman, P. A. *J. Phys. Chem.* **1993**, *97*, 10269–10280.

(47) Cornell, W. D.; Cieplak, P.; Bayly, C. I.; ; Kollmann, P. A. *J. Am. Chem. Soc.* **1993**, *115*, 9620–9631.

(48) Tao, P.; Fisher, J. F.; Shi, Q.; Vreven, T.; Mobashery, S.; Schlegel, H. B. *Biochemistry* **2009**, *48*, 9839–9847.

(49) Morokuma, K.; Wang, Q.; Vreven, T. *J. Chem. Theory Comput.* **2006**, *2*, 1317–1324.

(50) Tao, P.; Fisher, J. F.; Shi, Q.; Mobashery, S.; Schlegel, H. B. *J. Phys. Chem. B* **2010**, *114*, 1030–1037.

(51) Zhou, J.; Tao, P.; Fisher, J. F.; Shi, Q.; Mobashery, S.; Schlegel, H. B. *J. Chem. Theory Comput.* **2010**, *6*, 3580–3587.

(52) R.Rutledge, L.; Wetmore, S. D. *J. Am. Chem. Soc.* **2011**, *113*, 16258–16269.

(53) Haines, B. E.; Steussy, C. N.; Stauffacher, C. V.; Wiest, O. *Biochemistry* **2012**, *51*, 7893–7995.

(54) Ding, L.; Chung, L. W.; Morokuma, K. *J. Phys. Chem. B* **2013**, *117*, 1075–1084.

(55) Sumner, S.; Soderhjlem, P.; Ryde, U. *J. Chem. Theory Comput.* **2013**, *9*, 4205–4214.

(56) Stites, W. E.; Pranata, J. *Proteins* **1995**, *22*, 132–140.

(57) Wilson, K. A.; Baer, S.; Maerz, A. L.; Alizon, M.; Poumbourios, P. *J. Virol.* **2005**, *79*, 4533–4539.

(58) Wilson, K. A.; Maerz, A. L.; Baer, S.; Drummer, H. E.; Poumbourios, P. *Biochem. Biophys. Res. Commun.* **2007**, *359*, 1037–1043.

(59) Baumann, T.; Kaempfer, U.; Schuerch, S.; Schaller, J.; Largiader, C.; Nentwig, W.; Kuhn-Nentwig, L. *Cell Mol. Life Sci.* **2010**, *67*, 2787–2798.

(60) Harrison, C. F.; Lawson, V. A.; Coleman, B. M.; Kim, Y. S.; Masters, C. L.; Cappai, R.; Barnham, K. J.; Hill, A. F. *J. Biol. Chem.* **2010**, *285*, 20213–20223.

(61) Gracia-Volica, M.; Gao, J.; Karplus, M.; Truhlar, D. G. *Science* **2004**, *303*, 186–194.

(62) Hammes, G. G. *Biochemistry* **2002**, *41*, 8221–8228.

(63) Peraro, M. D.; Vila, A. J.; Carloni, P.; Klein, M. L. *J. Am. Chem. Soc.* **2007**, *129*, 2808–2816.

(64) Bhabha, G.; Lee, J.; Ekiert, D.; Gam, J.; Wilson, I.; Dyson, H.; Benkovic, S.; Wright, P. *Science* **2011**, *332*, 234–238.

(65) Mesecar, A. D.; Stoddard, B. L.; Koshland, D. E. *Science* **1997**, *277*, 202–206.

(66) Falke, J. *Science* **2002**, *295*, 1480–1481.

(67) Benkovic, S.; Hammes-Schiffer, S. *Science* **2003**, *301*, 1196–1202.